analytical chemistry

Article

pubs.acs.org/ac

From Electrochemistry to Electroluminescence: Development and Application in a Ratiometric Aptasensor for Aflatoxin B1

Long Wu,[†] Fan Ding,[†] Wenmin Yin, Jing Ma, Biru Wang, Axiu Nie, and Heyou Han*

State Key Laboratory of Agricultural Microbiology, College of Food Science and Technology, College of Science, Huazhong Agricultural University, Wuhan 430070, People's Republic of China

Supporting Information

ABSTRACT: Aflatoxin B1 (AFB1), one of the most toxic chemical carcinogens, has been widely studied. It remains challenging to develop simple, accurate, and sensitive analytical methods for the detection of AFB1 in food matrixes. In this work, on the basis of a dual-signaling strategy, a ratiometric aptasensor was designed and verified for the accurate and sensitive detection of AFB1. The electrochemical method was first used as a model to verify the specific interaction between AFB1 and the aptamer, in which ferrocene (Fc)-anchored and methylene blue (MB)-anchored DNA sequences acted as dual signals. Consequently, the specific interaction between AFB1 and its aptamer was demonstrated by the "signal-on" mode of Fc and the "signal-off" mode of MB. Due to the simple dual-signaling mode, the electrochemical sensor was further extended to the construction of an electrochemiluminoscence (ECL) aptasensor. In the ECL system, dual ECL signals were produced from CdTe/CdS/ZnS quantum dots (QDs) and luminol. Horseradish peroxidase-modified gold nanorods (HRP/Au NRs) acted as the quencher/enhancer and as such quenched the ECL signal of the QDs by ECL energy transfer and simultaneously catalyzed H_2O_2 to enhance the ECL of luminol. Owing to the self-calibration by the internal reference, both of the ratiometric aptasensors exhibited accurate and sensitive analytical performance for AFB1 with a good linear range from 5.0 pM to 10 nM and detection limits of 0.43 and 0.12 pM (S/N = 3), respectively. The aptasensors also exhibited good selectivity, reproducibility, and stability, revealing potential applications in food safety monitoring and environmental analysis.

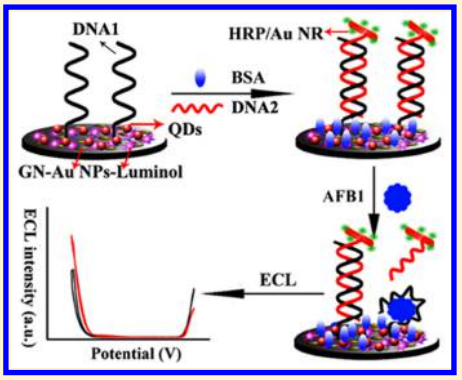

As far as food analysis is concerned, food safety has been considered as a major issue worldwide and a priority of governmental affairs.[1,2] Mycotoxins, a type of toxic secondary metabolites produced by fungi, are extensively found in foodstuffs with a wide range of toxic effects.[3] Owing to the potential adverse effects on humans, the research on mycotoxins has been intensively reported.[4,5] Among mycotoxins, aflatoxins have attracted the most attention because they are highly toxic natural compounds which can contaminate many food products such as grain, wine, peanut, and soy products.[6,7] Commonly, aflatoxins are divided into different types, such as B1, B2, G1, G2, M1, and M2.[8,9] Among them, aflatoxin B1 (AFB1), produced by molds such as *Aspergillus flavus* and *Aspergillus parasiticus*, is the most toxic in known chemical carcinogens.[10,11] Moreover, it was reported that exposure to AFB1 may cause severe disease such as liver cirrhosis, necrosis, and carcinoma in human beings and animals.[12] Therefore, it is of great significance to construct sensitive and reliable analytical methods for the determination of trace AFB1.

Until now, analytical approaches for the detection of AFB1 have been mainly focused on chromatography techniques and immunoassay.[13] Due to their accuracy and sensitivity, chromatography methods such as high-performance liquid chromatography (HPLC) and liquid chromatography–mass spectrometry (LC–MS) are the commonly used methods in AFB1 detection.[14] However, these techniques require complicated procedures and heavy instrumentation, which are not suitable for the analysis of multiple samples and on-site detection.[15,16] Immunoassay-based analytical methods, such as enzyme-linked immunosorbent assay (ELISA), immunochromatographic assays, and immunosensors, have been widely utilized for the rapid determination of AFB1 in food products.[17−19] Though these methods possess high sensitivity and selectivity, they often require a long reaction time and a complex operation process.[20] In addition, the involved antibodies and enzymes suffer from disadvantages such as a high cost of production and ease of denaturing during storage.[21] Thus, it is highly meaningful to develop a simple, rapid, and low-cost method for the detection of AFB1 in food matrixes.[22]

Aptamers, a type of small single-stranded oligonucleotides, can bind to target molecules with high affinity and selectivity and are comparable to antibodies. Also, when compared with antibodies, the production of aptamers is less expensive and labor-intensive and it is easier for them to be modified with fluorescent dyes, enzymes, and biotin.[23] In this context,

Received: April 13, 2017
Accepted: June 23, 2017
Published: June 23, 2017

DOI: 10.1021/acs.analchem.7b01399
Anal. Chem. 2017, 89, 7578−7585

Scheme 1. Schematic Illustration of the Dual-Signaling Sensor for AFB1 Assay with (A) Electrochemistry and (B) Electrochemiluminoscence[a]

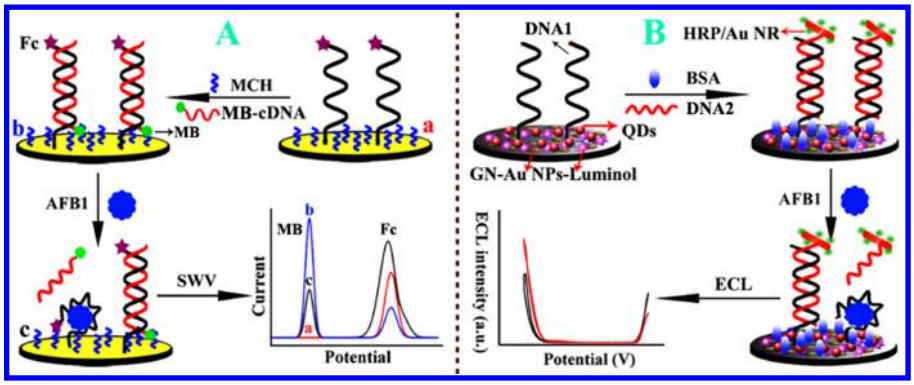

[a]Fc = ferrocene, MB = methylene blue, MCH = 6-mercaptohexanol, and AFB1 = aflatoxin B1.

aptamers have been intensively adopted to develop potential analytical tools to obtain the desired portability and high sensitivity and specificity.[24−26] Combining sensitivity and the advantages of electrochemical detection, electrochemical aptasensors exhibit very promising performance, which was proved by commercial glucose sensors with the specific recognition of the target analyte.[1,27] Furthermore, electrochemical aptasensors have the advantages of requiring small amounts of samples and being miniaturized.[28] However, most of the reported electrochemical aptasensors for AFB1 detection were based on only one signal, either the "signal-on" or "signal-off" mode, which may suffer from the signal fluctuation caused by variations in the detection system and some external factors.[29−31] Therefore, the dual-signaling electrochemical strategy was developed to avoid the limited signaling capacity of the one-signal strategy.[32] Usually, two different redox tag-labeled DNA strands were utilized to produce dual signals. The dual-signaling strategy exhibits better analytical performance such as a lower detection limit and higher accuracy and reproducibility than the single-signaling strategy.[33−35] Though the dual-signal strategy can achieve superior electrochemical performance to some extent, many target analytes such as bisphenol A and AFB1 themselves possess redox activity, which could provide an additional signal and thus may disturb the signal response of tag-labeled DNA strands.[36,37] Inspired by the above facts, we focused our work on developing a new electrochemical dual-signaling aptasensor and extended it to electrochemiluminoscence (ECL) for AFB1 detection in food samples.

In this work, a simple electrochemical dual-signaling strategy was explored and then extended to the ECL for accurate and sensitive detection of AFB1 in the food matrixes. As shown in Scheme 1A, the sensing system was first constructed and verified by using a ferrocene (Fc)-labeled AFB1 aptamer probe (Fc-P) to bind with methylene blue (MB)-labeled complementary DNA (MB-cDNA). After the specific recognition of AFB1 with Fc-P, MB-cDNA was released from the electrode surface and the Fc tag of the aptamer sequences came close to the electrode surface due to their conformational change.[38] As a result, the electrochemical signal of MB exhibited a decrement and Fc showed an increment. This conformational change of the aptamer can be extended to the ECL system, where ECL signals were produced from CdTe/CdS/ZnS quantum dots (QDs) and luminol (Scheme 1B). Therein, horseradish peroxidase-modified gold nanorods (HRP/Au NRs) acted as the quencher/enhancer and as such quenched the ECL signal of the QDs and simultaneously catalyzed H_2O_2 to enhance the ECL intensity of luminol. In the absence of AFB1, both the ECL signal of the QDs and luminol appeared as the cDNA hybridized with the aptamer. If the target exists, the AFB1 aptamers will hybridize with the target and release the cDNA sequence, which leads to the increment of the QD ECL signal and the decrease of the luminol signal. The ratio of the ECL intensity (QDs/luminol) exhibited a good linearity and high sensitivity for AFB1 detection. Due to the self-calibration by the internal reference, the method could produce accurate results. Thus, the ratiometric ECL sensor is expected to be a useful analytical tool for AFB1 detection in food and environmental monitoring.

EXPERIMENTAL SECTION

Chemical Reagents. Aflatoxin B1 (AFB1), aflatoxin B2 (AFB2), aflatoxin G1 (AFG1), aflatoxin G2 (AFG2), aflatoxin M1 (AFM1), deoxynivalenol (DON), zearalenone (ZON), bovine serum albumin (BSA), cetyltrimethylammonium bromide (CTAB; 99%), tris(2-carboxyethyl)phosphine hydrochloride solution (TCEP), and poly(diallyldimethylammonium chloride) (PDDA) were obtained from Sigma-Aldrich. Hydrogen peroxide (H_2O_2; 30%), sodium borohydride ($NaBH_4$), chloroauric acid ($HAuCl_4{\cdot}3H_2O$; AR), graphite powder, chitosan, glutaraldehyde (2.5%), ascorbic acid (AA), and silver nitrate ($AgNO_3$) were obtained from Sinopharm Chemistry Reagent Co., Ltd. (Shanghai, China). Horseradish peroxidase (HRP) was acquired from Shanghai Dongfeng Biochemical Technology Co., Ltd. CdTe/CdS/ZnS quantum dots (QDs; 660 ± 10 nm) were purchased from Xingzi (Shanghai) New Material Technology Development Co., Ltd. AFB1 aptamer and related DNA sequences used in this work (Table S1) were purchased from Wuhan Gene Create Biological Engineering Co., Ltd. (Wuhan, China). All other solvents were of analytical grade and were used without further treatment. Ultrapure water was used throughout the experiments to prepare aqueous solutions (resistance 18.2 MΩ cm).

Apparatuses. Photoluminescence (PL) spectra were performed on an Edinburgh FLS920 spectrometer with an integrating-sphere attachment. UV−vis absorption spectra were acquired via a Nicolet Evolution 300 UV−vis spectrometer (Thermo Nicolet, United States). Fourier-transform infrared (FT-IR) spectra were obtained on a Nicolet Avatar-330 spectrometer with 4 cm^{-1} resolution using the KBr pellet

DOI: 10.1021/acs.analchem.7b01399
Anal. Chem. 2017, 89, 7578−7585

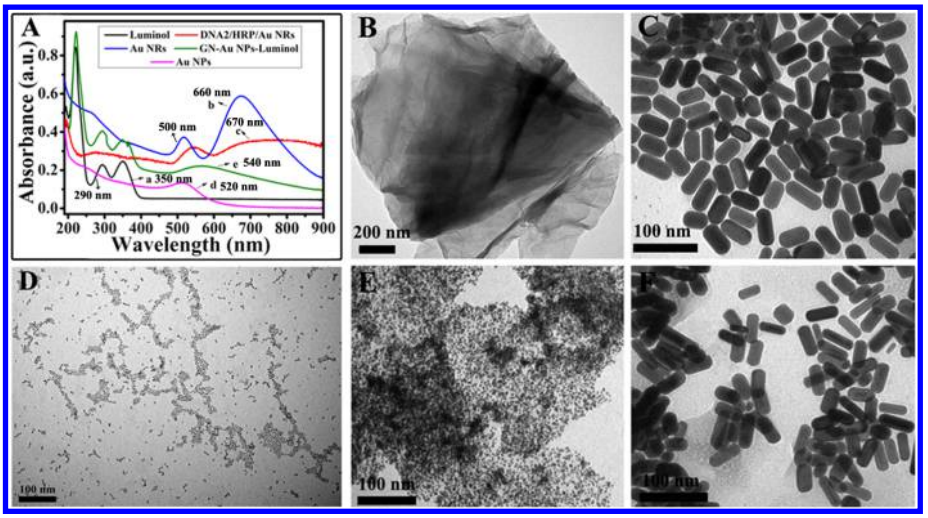

Figure 1. (A) UV−vis absorption spectra of (a) luminol, (b) Au NRs, (c) DNA2/H/Au, (d) Au NPs, and (e) GN−Au−L hybrids. TEM images of (B) GN, (C) Au NRs, (D) Au NPs, (E) GN−Au−L hybrids, and (F) DNA2/H/Au.

technique. The ζ potential and hydrodynamic size were measured by dynamic light scattering (DLS) using a Malvern Zetasizer (Nano-ZS) system. Transmission electron microscopy (TEM) images were taken with a JEM-2010 transmission electron microscope. The results of electrochemical impedance spectroscopy (EIS), cyclic voltammetry (CV), and square-wave voltammetry (SWV) were obtained on an electrochemical workstation (CHI 660E, CH Instrument Co., Shanghai). ECL emission spectra were acquired from a model MPI-EII ECL analyzer (Xi'an Remex Electronic Science and Technology Co. Ltd., China). All electrochemical experiments were performed via a conventional three-electrode system, and an Ag/AgCl (saturated KCl) electrode was used as the reference electrode.

Preparation of GN−Au NP−Luminol Hybrids. Au NPs and graphene (GN) were first synthesized on the basis of the previous work.[39] After that, 100 μL of the PDDA−GN (0.1 mg mL^{-1}) was mixed with 3 mL of Au NP solution (0.1 mg mL^{-1}) under stirring, followed by addition of 250 μL of luminol (10 mM), and then the mixture was sonicated for about 30 min to obtain a homogeneous solution. Next, the mixture was kept still under ambient conditions overnight to allow it to completely self-assemble. Finally, after centrifugation, the supernatant was discarded and the precipitate was collected and washed with water three times. The obtained GN−Au NP−luminol hybrids (GN−Au−L) were suspended in water for further use.

Preparation of DNA2/HRP/Au NR Composites. Gold nanorods (Au NRs) were synthesized on the basis of previous work with some changes.[40,41] Then the HRP/Au NR hybrids were prepared according to Wen's report.[42] Simply, the obtained Au NR solution was first centrifuged at 12000 rpm for 15 min, and the precipitation was redispersed in water to remove extra free CTAB. Next, 40 μL of 5 μM DNA2 solution and 100 μL of 200 μM TCEP were introduced to 500 μL of Au NR solution. After the solution was shaken for 1 h at room temperature, its pH was adjusted by adding 0.1 M NaOH (0.7 μL). Finally, 80 μL of HRP (1 mg mL^{-1}) was mixed with the above solution and the resulting solution incubated for 1.5 h by shaking at room temperature. Then the temperature was adjusted to 4 °C for 4 h to obtain stable DNA2/HRP/Au NR composites (DNA2/H/Au). The mixture was washed by centrifugation at 12000 rpm for 15 min to remove excess reagents.

Construction of the AFB1 Sensor. The pretreatment of electrodes was the same as that in our previous works (Supporting Information).[43,44] Then a gold electrode (GE) was immersed into 0.1 M phosphate-buffered saline (PBS; pH 7.0) containing 5 μM Fc-P for 24 h at 4 °C to form a self-assembled Fc-P monolayer. After that, the unreacted electrode surface was subsequently blocked by incubation with 6-mercaptohexanol (MCH; 2 mM) for 1 h and then washed thoroughly with Tris−HCl solution (10 mM, pH 7.4). Finally, 10 μL of MB-cDNA solution (10 μM) was dropped onto the Au electrode to obtain the DNA duplex via base pairing (Scheme 1A). To verify each modification step, CV and EIS were performed in the solution of 0.5 M KCl containing 5 mM $K_3[Fe(CN)_6]$ with a frequency range of 1−10^5 Hz and a signal amplitude of 5 mV. All the as-prepared electrodes were stored at 4 °C when not in use.

For the construction of the ECL AFB1 sensor, 5 μL of GN−Au−L hybrids was cast onto the glass carbon electrode (GCE) and dried in air to produce the GN−Au−L-modified electrode (GN−Au−L/GCE). Subsequently, 2 μL of CdTe/CdS/ZnS QDs was dropped onto the GN−Au−L/GCE surface, followed by addition of 5 μL of chitosan (0.05 wt %) to stabilize the electrode (Scheme 1B). After that, 6 μL of glutaraldehyde was drop-cast onto QDs/GN−Au−L/GCE for DNA immobilization.[45] Next, 5 μL of AFB1 aptamer (DNA1) was introduced to cross-link onto the glutaraldehyde-modified electrode at 4 °C overnight. Then 2.5 μL of BSA (0.5%) was introduced to block the unreacted electrode surface, and the GCE was washed with PBS to remove excess reactants. Finally, DNA2/H/Au composites were added to hybridize with the AFB1 aptamer. Other control electrodes used in the experiments were prepared with similar procedures.

Electrochemical Measurements. To obtain the linear calibration curves of AFB1, the prepared Au electrode was incubated with various concentrations of AFB1 for 3 h. Then the electrode was rinsed thoroughly in the Tris−HCl solution (10 mM, pH 7.4) three times to wash away the unbound AFB1 and the released MB-cDNA. The obtained electrode was immersed into 0.1 M PBS (pH 7.4) containing 0.1 M KCl and investigated by CV and SWV. The control experiments for aflatoxin B2 (AFB2), aflatoxin G1 (AFG1), aflatoxin G2 (AFG2), aflatoxin M1 (AFM1), deoxynivalenol (DON), and

DOI: 10.1021/acs.analchem.7b01399
Anal. Chem. 2017, 89, 7578−7585

zearalenone (ZON) were performed at the same conditions. All experiments were performed at room temperature and measured three times.

ECL Characterization Assays. The modified GCE electrodes were characterized by ECL measurements in 0.1 M PBS (pH 7.4) containing H_2O_2 (10 mM) with the conventional three-electrode system. The ECL measurements were carried out from −1.6 to 0.6 V at a scan rate of 300 mV s^{-1}.[46] The ECL detection procedures for AFB1 and the control experiments were the same as those for the electrochemical measurements.

RESULTS AND DISCUSSION

Characterization of the GN−Au−L Hybrids and DNA2/H/Au Composites. FT-IR spectroscopic and UV−vis absorption experiments were first carried out to investigate the synthesized materials. As shown in Figure S1A (Supporting Information), the absorption bands at 2329 cm^{-1} (CH_n), 1650 cm^{-1} (C═O), and 1380 cm^{-1} (C═C) corresponded to the characteristic bands of GN−PDDA, which revealed the successful modification of PDDA with GN. For the spectrum of GN−Au−L, two characteristic peaks of luminol appeared at 3030 and 825 cm^{-1}. As depicted in Figure S1B, DNA2/H/Au displayed absorption bands at 2904, 2850, 1650, 1510, and 1050 cm^{-1}, revealing the successful conjugation of HRP and DNA2. In addition, the above materials were confirmed by UV−vis analysis as shown in Figure 1A. GN−Au−L hybrids exhibited several strong characteristic absorption peaks at 270, 540, and 290 and 350 nm, which were attributed to the absorbance of GN, Au NPs, and luminol, respectively. The red-shifted peak of Au NPs at 540 nm further indicated the efficient adsorption of Au NPs onto the GN surface. Notably, Au NRs showed two plasmon resonances, a transverse plasmon (~510 nm) and a longitudinal plasmon (~660 nm). After modification with HRP and DNA2, the two peaks were shifted to ~520 and ~680 nm and the longitudinal plasmon showed a wide absorbance band. Moreover, TEM images of GN before (Figure 1B) and after (Figure 1E) hybridization with Au NPs (Figure 1D) and luminol also demonstrated the formation of the GN−Au−L hybrids. From Figure 1E, it was observed that numerous Au NPs are decorated on the surface of GN. As shown in Figure 1C, the monodispersed Au NRs possessed an aspect ratio of ~3 with an average diameter of ~16 nm and average length of ~50 nm. According to Figure 1F, it can be clearly observed that DNA2 and HRP were conjugated on Au NRs and formed the DNA2/H/Au composites. The above characterization results indicated that the materials in Scheme 1B were synthesized as desired.

Moreover, the ζ potentials of the DNA2/H/Au composites and GN−Au−L hybrids were also explored (Figure 2). As presented in Figure 2A, the ζ potential of the Au NRs showed a positive surface charge of +32.7 mV but a negative surface charge of −18.2 mV for DNA2/H/Au. Meanwhile, before and after the modification of GN, the ζ potential varied from +25.8 mV (GN) to −10.5 mV (GN−Au−L). The variations of the ζ potential demonstrated the successful fabrication of GN−Au−L hybrids and DNA2/H/Au composites. Additionally, PL spectra were adopted to characterize the fluorescence properties of GN−Au−L (Figure 2B). The PL emission peak of the QDs was at 650 nm with a red-emitting light (curve a) and that of luminol at 435 nm with a blue emitting light (curve b). After the QDs and luminol were mixed with GN−Au NPs and GN−Au−L hybrids, their emission peaks exhibited a red shift to ~660 and ~440 nm, respectively (curves c and d). In addition,

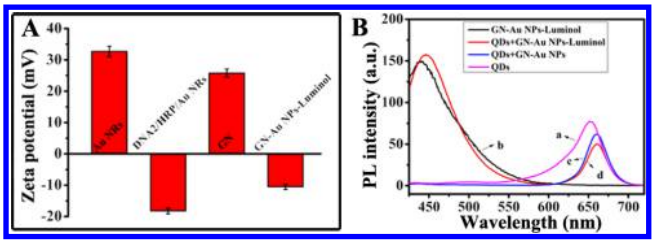

Figure 2. (A) ζ potential measurements of Au NRs, DNA2/HRP/Au NR composites, GN, and GN−Au NP−luminol hybrids. (B) Fluorescence spectra of (a) QDs, (b) GN−Au NP−luminol hybrids, (c) QDs + GN−Au NPs, and (d) QDs + GN−Au NP−luminol hybrids.

the red shift and narrowed peak shape of the QDs were overlapped with the wide absorption peak of DNA2/H/Au (Figure 1A), which makes it possible for it to be a good energy donor for the receptor.

Characterization of the Aptasensor. First, the electrochemical experiments were performed to investigate the feasibility of the proposed SWV method for AFB1 assay. In this work, EIS and CV are adopted to characterize the modification process of the gold electrode (GE). It is well-known that the Niquist plot of EIS includes a semicircle portion and a linear portion, and the semicircle portion corresponds to the electron-transfer-limited process.[47,48] As shown in Figure S2A (Supporting Information), the bare GE shows a small semicircle domain (curve a), indicating a fast electron-transfer process. Due to the repulsion of negatively charged Fc-P with $[Fe(CN)_6]^{3-/4-}$anions (curve b), an enhanced electron-transfer resistance (R_{et}) is observed after incubation of Fc-P on the GE surface. Then the surface-blocking procedure with MCH further generates an enhancement of the R_{et} value (curve c). Next, the hybridization of Fc-P with MB-cDNA largely raises the R_{et} value to about 1400 Ω (curve d), which suggests the successful recognition of Fc-P and MB-cDNA. Finally, the R_{et} value of the corresponding electrode decreases after incubation with AFB1, which can be ascribed to the dissociation of the duplex and the release of MB-cDNA from the GE surface (curve e). Moreover, with the sequential assembly of Fc-P (curve b), blocking agent (curve c), and MB-cDNA (curve d), the current decreased steadily (Figure S2B). When the constructed sensor was incubated with AFB1, the current showed an increment (curve e). The results of CV are basically consistent with those of EIS, revealing that the sensing interface has been obtained according to Scheme 1A. The scan rate was also studied to explore the behavior of the modified electrode. It can be observed that the redox peaks change with the scan rate (Figure S2C), and the cathodic peak (curve a) and anodic peak (curve b) currents increase linearly as the scan rate increases (Figure S2D). The results showed that the electrochemical process is mainly controlled by adsorption rather than diffusion,[49] which agree with the fact that AFB1 is adsorbed onto the electrode surface by the aptamer (Scheme 1A).

The fabrication process for the ECL sensor was first characterized by the fluorescence microscopy (Figure S3, Supporting Information). The scattered fluorescence dots with blue (Figure S3A) and red (Figure S3B) color were observed clearly on the GN−Au−L/GCE and QDs/GCE, respectively. After the fabrication of QDs on GN−Au−L/GCE, the blue fluorescence of luminol was covered by the red fluorescence of the QDs (Figure S3C). Furthermore, with the modification of DNA1 and BSA, the fluorescence of the QDs

DOI: 10.1021/acs.analchem.7b01399
Anal. Chem. 2017, 89, 7578−7585

became a little dim due to the coverage (Figure S3D). After DNA2/H/Au was hybridized with DNA1/GN−Au−L, the fluorescence of the QDs highly darkened due to the quenching effects of DNA2/H/Au (Figure S3E). However, after incubation with AFB1, the fluorescence of the QDs became bright due to the dissociation of the DNA1/DNA2 duplex and the release of DNA2/H/Au (Figure S3F). These facts verified the successful assembly of the biosensor and confirmed the feasibility of modification repetition. In addition, the stepwise fabrication of the ECL aptasensor was demonstrated by CV and EIS. As shown in Figure 3A, a pair of symmetric redox peaks

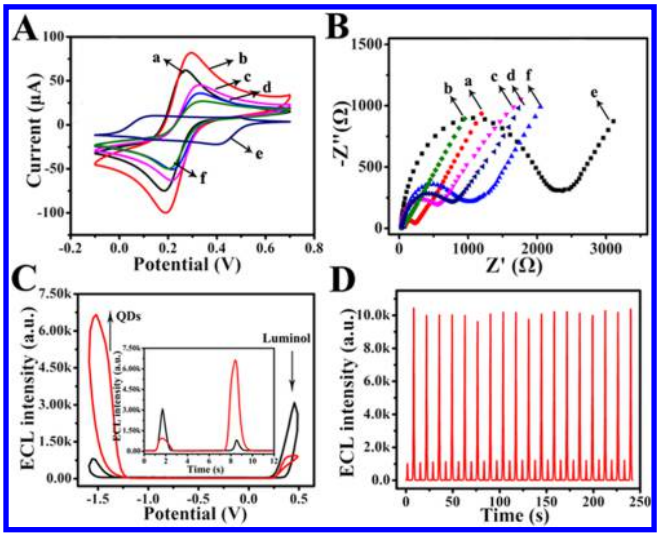

Figure 3. (A) CV curves and (B) EIS spectra of (a) the bare GCE, (b) GN−Au−L/GCE, (c) DNA1/QDs/GN−Au−L/GCE, (d) BSA/DNA1/QDs/GN−Au−L/GCE, (e) DNA2/H/Au/BSA/DNA1/QDs/GN−Au−L/GCE, and (f) AFB1/BSA/DNA1/QDs/GN−Au−L/GCE in a mixture solution of 1.0 mM $[Fe(CN)_6]^{3-/4-}$ and 0.1 M KCl. (C) ECL responses before and after incubation with AFB1 (10 nM). (D) Stability characterization of the ECL sensor for 240 s.

appeared corresponding to the reversible redox reaction of $[Fe(CN)_6]^{3-/4-}$ on the bare GCE (curve a). After the modification of GN−Au NPs, the peak current of the electrode increased clearly (curve b), implying that GN−Au NPs have a higher electrical conductivity. In the following stepwise assembly processes of QDs, BSA, DNA1, and DNA2/H/Au, the peak currents in the CV curves decreased successively (from curve c to curve e), which was caused by the lower conductivity of the materials and the electrostatic repulsion between the negative charge and the $[Fe(CN)_6]^{3-/4-}$ anion. However, when the sensor was incubated with AFB1, the current showed an obvious increment (from curve e to curve f), indicating the dissociation of the duplex and the release of DNA2/H/Au from the GCE surface. In addition, the assembly process was characterized by the Niquist plot of EIS to reveal the GCE surface features (Figure 3B). Due to the better electron-transfer capability of GN−Au NPs, the GN−Au−L/GCE exhibited a lower R_{et} than bare GCE (curves a and b). With the sequential assembly of DNA1 (curve c), BSA (curve d), and DNA2/H/Au (curve f), the R_{et} increased steadily. However, after incubation with AFB1, the R_{et} decreased dramatically (curve e). The results of EIS were accordance with those of CV, which confirmed the successful preparation of the ECL aptasensor (Scheme 1B).

The ECL aptamer sensor was further confirmed by ECL measurements (Figure 3C). A strong cathodic ECL signal (QDs) at −1.5 V and a weak anodic ECL signal (luminol) at +0.45 V can be observed simultaneously. Before the combination of DNA2/H/Au, the ECL intensity of the QDs was much higher than that of luminol and the ECL ratio of luminol/QDs was calculated to be about 1:8. However, after connection with the DNA2/H/Au probe, the ECL peak of luminol was higher than that of the QDs and the ECL ratio of luminol/QDs was calculated to be 4:1, which was ascribed to the HRP catalytic reactions and the quenching from DNA2/H/Au. The results revealed that the ECL ratiometric aptasensor was successfully constructed. In addition, the ECL process and possible mechanism of the dual-potential ECL are presented in Figure S4 (Supporting Information). Also, the signal stability of the ECL ratiometric aptasensor in the ECL measurements was explored and is displayed in Figure 3D. After incubation with 1 nM AFB1 solution for 2 h, the ECL intensities of the aptasensor still remained at a stable value (4.8% variation) under testing for 40 cycles, indicating the acceptable stability of the ratiometric aptasensor. To further verify the acceptable stability and reproducibility, the results were compared with those from other work and are listed in Table S2 (Supporting Information).

Influencing Factors on the Aptasensor. To obtain the best analytical performance of the developed aptasensor, different parameters such as pH, Fc-P concentration, hybridization time, and incubation time were explored for the electrochemical sensor as a model. The effect of the pH on the current changes for the detection of 0.1 nM AFB1 was first studied (Figure S5A, Supporting Information). It is observed that the maximum current appeared when the pH value was 7.4. Hence, 7.4 was chosen as the optimal pH for the following experiments. As shown in Figure S5B, the current increased with increasing Fc-P concentration and reached the highest when the Fc-P concentration was 5 μM. Thus, the aptasensor was constructed with 5 μM Fc-P. In addition, the hybridization time for MB-cDNA and Fc-P was also studied (Figure S5C). The current value of I_{MB} increased with increasing hybridization time and tended to be balanced at 4 h, which suggested the saturated hybridization between MB-P and Fc-P. Similarly, the incubation time showed the same trends as the hybridization time and reached a plateau at 4 h (Figure S5D). Thus, the optimum hybridization and incubation times were chosen as 4 h for the sensor.

Characterization of the Electrochemical Detection of AFB1. Prior to the AFB1 detection, CV and SWV measurements were performed to determine the performance of the electrochemical sensor. As shown in Figure 4A, Fc-P/GE showed an anodic peak current at ~0.3 mV corresponding to

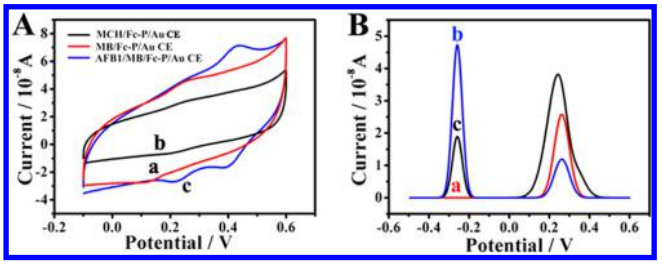

Figure 4. (A) CV and (B) SWV measurements of (a) Fc-P/GE, (b) MB-cDNA/Fc-P/GE, and (c) AFB1/Fc-P/GE.

DOI: 10.1021/acs.analchem.7b01399
Anal. Chem. 2017, 89, 7578−7585

the oxidation peak of Fc (curve a). After the hybridization with MB-cDNA, the current of Fc dramatically dropped, indicating the successful formation of an Fc-P/MB-P DNA duplex (curve b). When MB-cDNA/Fc-P/GE was further incubated with AFB1, the current of Fc increased, and at the same time, a new peak of AFB1 appeared at ~0.4 mV (curve c). The same results were verified by SWV measurements as shown in Figure 4B. A single oxidation peak of Fc for Fc-P/GE (curve a) can be seen. A new peak was produced at ~−0.3 mV and the current of Fc decreased when Fc-P/GE was incubated with MB-cDNA (curve b), which can be due to the fact that the Fc-P tail is far away from the electrode surface. After incubation with AFB1, the peak current of MB decreased and that of Fc significantly increased with a wider peak shape (curve c), revealing that AFB1 was hybridized with the aptamer and provided an additional signal overlapping with the peak of Fc.

Determination of AFB1. On the basis of the above optimized conditions, the analytical performance of the aptasensor was first investigated by SWV. As shown in Figure 5A, with increasing concentration of AFB1 (from 1.0 pM to 50 nM), the current of Fc (I_{Fc}) gradually increased and that of MB (I_{MB}) decreased simultaneously, which indicated the good capability of the aptasensor in response to the target. Figure 5B displays the current plots of different concentrations of AFB1 corresponding to Figure 5A. It can be seen that the greater the amount of AFB1, the more I_{Fc} increased and I_{MB} decreased, and both of them reached a plateau at 50 nM AFB1, which revealed that the combination between AFB1 and its aptamer was saturated. Figure 5C shows that the current was dependent on the logarithm of the AFB1 concentration (C_{AFB1}) with the respective calibration curves of I_{Fc} and I_{MB}. The limits of detection (S/N = 3) of I_{Fc} and I_{MB} were estimated to be 1.2 pM (R = 0.9286) and 4.6 pM (R = 0.9783). To prove the superior precision of the aptasensor, plots of the dual-signal fluorescence intensity ratio were described (Figure 5D). They showed that the value of I_{MB}/I_{Fc} linearly corresponded to the logarithm of C_{AFB1} from 1.0 pM to 50 nM (Figure 5D). The linear regression equation was $Y = -1.3480X + 1.8296$ with R = 0.9889, and the limit of detection (LOD) was estimated to be 0.43 pM (S/N = 3), where Y is the I_{MB}/I_{Fc} ratio and X is the logarithm of C_{AFB1}. The results revealed that the dual-signal mode has a lower error and signal fluctuation and a higher sensitivity and R value, demonstrating the superiority of the ratiometric aptasensor.

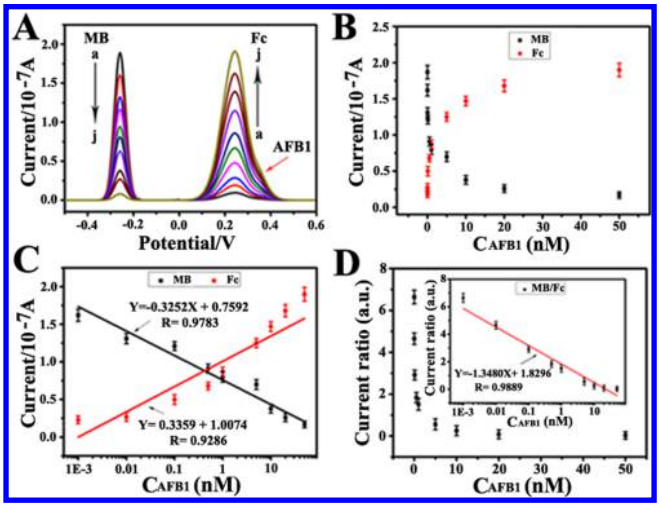

Figure 5. (A) Detection results of different C_{AFB1} values based on SWV measurements (from curve a to curve j, 0, 0.001, 0.01, 0.1, 0.5, 1, 5, 10, 20, and 50 nM). (B) Current plots of different C_{AFB1} values (from 1.0 pM to 50 nM) corresponding to the results of (A). (C) Calibration curve of I_{MB} and I_{Fc} for the detection of AFB1. (D) Dual-signaling I_{MB}/I_{Fc} current intensity ratio (inset: calibration curve of I_{MB}/I_{Fc} for determining different C_{AFB1} values ranging from 1.0 pM to 50 nM). All the error bars were calculated on the basis of the standard deviation of three measurements.

Considering that AFB1 may have effects on the Fc current, the dual-signal mode was further studied by the ECL aptasensor (Figure 6). As depicted in Figure 6A, it can be clearly observed that the ECL signal of the QDs increased and that of luminol decreased with an increase of C_{AFB1}. In addition, the $ECL_{QDs}/ECL_{luminol}$ raio was linearly dependent on the logarithm of C_{AFB1} in the range from 5.0 pM to 10 nM (Figure 6B). The linear regression equation was $Y = 4.3701X + 1.8820$ with R = 0.9920, and the LOD was estimated to be 0.12 pM (S/N = 3), where Y is the $ECL_{QDs}/ECL_{luminol}$ ratio and X is the logarithm of C_{AFB1}. Figure 6C shows the plots of the dual-signal ratio of the ECL intensity, which confirmed the good linear relation between the logarithm of C_{AFB1} and the ECL intensity ratio. Parts D and E of Figure 6 exhibit the ECL single-signal results and the calibration curves of ECL_{QDs} and $ECL_{luminol}$, and their LODs were estimated to be 1.8 pM (R = 0.9891) and 2.1 pM (R = 0.9529), respectively. The results demonstrated that the ratiometric ECL aptasensor also owns a lower error and signal fluctuation and a higher sensitivity and R value than the single-signal ECL method. From the results of electrochemical measurements and the ECL aptasensor, it can be concluded that both electrochemistry and the ECL ratiometric aptasensor have good analytical performance toward AFB1. Moreover, the proposed electrochemical measurements and ECL aptasensor were compared with other methods in previously published reports (Table S3, Supporting Information). It can be seen that both methods exhibit a higher sensitivity than other previously reported methods, which further reveals the superiority of the proposed method in the determination of AFB1.

Specificity, Reproducibility, and Stability of the Aptasensor. The specificity of the aptasensor for AFB1 was investigated by taking equal amounts of AFB2, AFG1, AFG2, AFM1, DON, and ZON as interfering agents. As shown in Figure 6F, only in the presence of AFB1 was the large $ECL_{QDs}/ECL_{luminol}$ ratio observed, and the interfering agents had no obvious effect on the ratios of the ECL intensity, revealing the excellent specificity of the ECL ratiometric aptasensor. The reproducibility was demonstrated with an intra-assay by measuring the same level of AFB1 (0.5 nM) for five measurements. The coefficient of variation (CV) was 4.8%, indicating the acceptable reproducibility of the ECL aptasensor. In addition, it was found that the aptasensor remained at 90% of the original ECL signal after 10 days of storage at 4 °C, revealing the acceptable stability of the biosensor.

Real Sample Analysis. To evaluate the potential application of the proposed method, the ECL ratiometric aptasensor was used in the detection of real food samples (Figure S6, Supporting Information). The extraction procedures for the food samples are elaborated in the Supporting Information. The standard addition method was utilized to analyze food samples, and the relative standard deviation (RSD) was adopted to evaluate the accuracy and precision of the results. The results are displayed in Table 1, and the samples were spiked with standard AFB1 at 1, 2, and 5 nM for

DOI: 10.1021/acs.analchem.7b01399
Anal. Chem. 2017, 89, 7578−7585

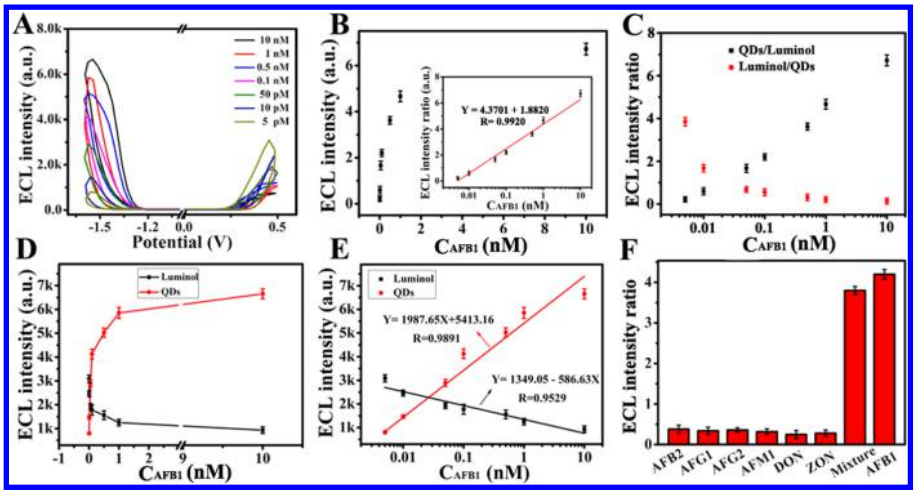

Figure 6. (A) Detection results of different C_{AFB1} values based on the ECL sensor (from curve a to curve j, 0.005, 0.01, 0.05, 0.1, 0.5, 1, and 10 nM). (B) Dual-signaling ECL intensity ratio of $I_{QDs}/I_{Luminol}$ (inset: calibration curve of ECL $I_{QDs}/I_{luminol}$ for different C_{AFB1} values from 5.0 pM to 10 nM). (C) Dual-signaling ECL intensity ratio of QDs and luminol. (D) Single-signaling ECL intensities of QDs and luminol. (E) Calibration curve of ECL luminol and ECL QDs for determining different C_{AFB1} values (5.0 pM to 10 nM) in 0.1 M pH 7.4 PBS. (F) Specificity of the ECL ratiometric aptasensor to AFB1 (0.5 nM) by comparison with AFB2, AFG1, AFG2, AFM1, DON, and ZON (1 nM) and their mixture (AFB1:AFB2:AFG1:AFG2:AFM1:DON:ZON = 1:1:1:1:1:1:1:1). All the error bars were calculated on the basis of the standard deviation of three measurements.

Table 1. Results of the Determination of AFB1 in Real Food Samples and Recovery Test

sample	found (nM)	added (nM)	found (mg/L)	recovery, RSD (n = 3, %)
peanut	0.48	1.0	1.54	106, 4.8
		2.0	2.63	107.5, 5.2
		5.0	5.14	93.2, 3.9
maize	0.25	1.0	1.36	111, 3.8
		2.0	2.19	97, 4.6
		5.0	5. 48	104.6, 5.0
wheat	0.08	1.0	1.15	107, 4.8
		2.0	2.16	104, 4.0
		5.0	5.02	98.8, 2.7

the recovery test, respectively. The three kinds of food samples (peanut, maize, and wheat) were evaluated, and no AFB1 was found in the clean samples. However, as shown in Table 1, the moldy food samples were all found with a trace of AFB1 and, after the addition of standard AFB1, the recoveries and RSDs were in the range of 93.2−111% and 2.7−5.2%, respectively, indicating that the ECL ratiometric aptasensor has good accuracy and is acceptable for food sample analysis.

CONCLUSION

In this work, an electrochemical ratiometric aptasensor was designed and verified for the accurate and sensitive detection of AFB1. Furthermore, the dual-signaling mode was extended to ECL on the basis of GN−Au−L hybrids, QDs, and DNA2/H/Au composites. QDs act as a donor and DNA2/H/Au acts as a receptor to realize ECL energy transfer. Owing to the high accuracy and sensitivity of the ratiometric aptasensor, both electrochemical measurements and the ECL sensor exhibited rapid, accurate, and sensitive recognition and determination of AFB1. Moreover, both of the ratiometric aptasensors exhibited accurate and sensitive analytical performance toward AFB1 with a good linear range and detection limits of 0.43 and 0.12 pM (S/N = 3), respectively. The aptasensor also exhibited good selectivity, reproducibility, and stability, revealing its potential applications in food safety monitoring, environmental analysis, and bioanalysis.

ASSOCIATED CONTENT

Supporting Information

The Supporting Information is available free of charge on the ACS Publications website at DOI: 10.1021/acs.analchem.7b01399.

Figures S1−S6 showing infrared spectra of the materials, electrochemical characterization of the sensor, fluorescence microscope images of luminol and QDs, a possible mechanism of the ECL sensor, effects of different conditions on the SWV measurements, and real food samples (PDF)

AUTHOR INFORMATION

Corresponding Author

*E-mail: hyhan@mail.hzau.edu.cn. Fax: (86)-027-8728 8505.

ORCID

Heyou Han: 0000-0001-9406-0722

Author Contributions

†L.W. and F.D. contributed equally to this work.

Notes

The authors declare no competing financial interest.

ACKNOWLEDGMENTS

We gratefully acknowledge the financial support from the National Key R&D Program (Grant 2016YFD0500700), National Natural Science Foundation of China (Grants 21375043 and 21175051), and Sci-tech Innovation Foundation of Huazhong Agriculture University (2662017PY042).

REFERENCES

(1) Vasilescu, A.; Marty, J. L. *TrAC, Trends Anal. Chem.* **2016**, *79*, 60−70.

(2) Wang, Y.; Duncan, T. V. *Curr. Opin. Biotechnol.* **2017**, *44*, 74−86.

DOI: 10.1021/acs.analchem.7b01399
Anal. Chem. 2017, 89, 7578−7585

(3) Marin, S.; Ramos, A. J.; Cano-Sancho, G.; Sanchis, V. *Food Chem. Toxicol.* **2013**, *60*, 218−237.
(4) Wu, F.; Groopman, J. D.; Pestka, J. J. *Annu. Rev. Food Sci. Technol.* **2014**, *5*, 351−372.
(5) Bezerra da Rocha, M. E.; Freire, F. d. C. O.; Maia, F. E. F.; Guedes, M. I. F.; Rondina, D. *Food Control* **2014**, *36*, 159−165.
(6) Shim, W. B.; Kim, M. J.; Mun, H.; Kim, M. G. *Biosens. Bioelectron.* **2014**, *62*, 288−294.
(7) Wang, X.; Pauli, J.; Niessner, R.; Resch-Genger, U.; Knopp, D. *Analyst* **2015**, *140*, 7305−7312.
(8) Li, P. W.; Zhang, Q.; Zhang, W. *TrAC, Trends Anal. Chem.* **2009**, *28*, 1115−1126.
(9) Bayram, E.; Yılmaz, E.; Uzun, L.; Say, R.; Denizli, A. *Food Chem.* **2017**, *221*, 829−837.
(10) Reddy, K. R. N.; Reddy, C. S.; Muralidharan, K. *Food Control* **2009**, *20*, 173−178.
(11) Hontanaya, C.; Meca, G.; Luciano, F. B.; Mañes, J.; Font, G. *Food Control* **2015**, *47*, 154−160.
(12) Bruix, J.; Boix, L.; Sala, M.; Llovet, J. M. *Cancer Cell* **2004**, *5*, 215−219.
(13) Tang, D.; Lin, Y.; Zhou, Q.; Lin, Y.; Li, P.; Niessner, R.; Knopp, D. *Anal. Chem.* **2014**, *86*, 11451−11458.
(14) Kong, W.; Wei, R.; Logrieco, A. F.; Wei, J.; Wen, J.; Xiao, X.; Yang, M. *Food Chem.* **2014**, *146*, 320−326.
(15) Shim, W. B.; Yang, Z. Y.; Kim, J. S.; Kim, J. Y.; Kang, S. J.; Woo, G. J.; Chung, Y. C.; Eremin, S. A.; Chung, D. H. *J. Microbiol. Biotechnol.* **2007**, *17*, 1629−1637.
(16) Togashi, M.; Terai, T.; Kojima, H.; Hanaoka, K.; Igarashi, K.; Hirata, Y.; Urano, Y.; Nagano, T. *Chem. Commun.* **2014**, *50*, 14946−14948.
(17) Mozaffari Nejad, A. S.; Sabouri Ghannad, M.; Kamkar, A. *Toxin Rev.* **2014**, *33*, 151−154.
(18) Ren, M.; Xu, H.; Huang, X.; Kuang, M.; Xiong, Y.; Xu, H.; Xu, Y.; Chen, H.; Wang, A. *ACS Appl. Mater. Interfaces* **2014**, *6*, 14215−14222.
(19) Xu, W.; Xiong, Y.; Lai, W.; Xu, Y.; Li, C.; Xie, M. *Biosens. Bioelectron.* **2014**, *56*, 144−150.
(20) Wang, B.; Chen, Y.; Wu, Y.; Weng, B.; Liu, Y.; Lu, Z.; Li, C. M.; Yu, C. *Biosens. Bioelectron.* **2016**, *78*, 23−30.
(21) Huang, Y.; Zhao, S.; Chen, Z. F.; Shi, M.; Liang, H. *Chem. Commun.* **2012**, *48*, 7480−7482.
(22) Lin, Y.; Zhou, Q.; Tang, D.; Niessner, R.; Yang, H.; Knopp, D. *Anal. Chem.* **2016**, *88*, 7858−7866.
(23) Famulok, M.; Mayer, G. *Acc. Chem. Res.* **2011**, *44*, 1349−1358.
(24) Wu, D.; Katilius, E.; Olivas, E.; Dumont Milutinovic, M.; Walt, D. R. *Anal. Chem.* **2016**, *88*, 8385−8389.
(25) Nguyen, V. T.; Seo, H. B.; Kim, B. C.; Kim, S. K.; Song, C. S.; Gu, M. B. *Biosens. Bioelectron.* **2016**, *86*, 293−300.
(26) Kim, U. J.; Kim, B. C. *Anal. Chim. Acta* **2016**, *936*, 208−215.
(27) Godman, N. P.; DeLuca, J. L.; McCollum, S. R.; Schmidtke, D. W.; Glatzhofer, D. T. *Langmuir* **2016**, *32*, 3541−3551.
(28) Mokhtarzadeh, A.; Ezzati Nazhad Dolatabadi, J.; Abnous, K.; de la Guardia, M.; Ramezani, M. *Biosens. Bioelectron.* **2015**, *68*, 95−106.
(29) Evtugyn, G.; Porfireva, A.; Stepanova, V.; Sitdikov, R.; Stoikov, I.; Nikolelis, D.; Hianik, T. *Electroanalysis* **2014**, *26*, 2100−2109.
(30) Lu, Z.; Chen, X.; Wang, Y.; Zheng, X.; Li, C. M. *Microchim. Acta* **2015**, *182*, 571−578.
(31) Castillo, G.; Spinella, K.; Poturnayová, A.; Šnejdárková, M.; Mosiello, L.; Hianik, T. *Food Control* **2015**, *52*, 9−18.
(32) Xiong, E.; Zhang, X.; Liu, Y.; Zhou, J.; Yu, P.; Li, X.; Chen, J. *Anal. Chem.* **2015**, *87*, 7291−7296.
(33) Liu, J.; Morris, M. D.; Macazo, F. C.; Schoukroun-Barnes, L. R.; White, R. J. *J. Electrochem. Soc.* **2014**, *161*, H301−H313.
(34) Wei, B.; Zhang, J.; Wang, H.; Xia, F. *Analyst* **2016**, *141*, 4313−4318.
(35) Zhang, H.; Dong, H.; Yang, G.; Chen, H.; Cai, C. *Anal. Chem.* **2016**, *88*, 11108−11114.
(36) Yu, P.; Liu, Y.; Zhang, X.; Zhou, J.; Xiong, E.; Li, X.; Chen, J. *Biosens. Bioelectron.* **2016**, *79*, 22−28.
(37) Zhu, Y.; Zhou, C. Q.; Yan, X. P.; Yan, Y.; Wang, Q. *Anal. Chim. Acta* **2015**, *883*, 81−89.
(38) Guo, X.; Wen, F.; Zheng, N.; Luo, Q.; Wang, H.; Wang, H.; Li, S.; Wang, J. *Biosens. Bioelectron.* **2014**, *56*, 340−344.
(39) Wu, L.; Yin, W.; Tang, K.; Li, D.; Shao, K.; Zuo, Y.; Ma, J.; Liu, J.; Han, H. *Anal. Chim. Acta* **2016**, *933*, 89−96.
(40) Nikoobakht, B.; El-Sayed, M. A. *Chem. Mater.* **2003**, *15*, 1957−1962.
(41) Wu, L.; Xiao, X.; Chen, K.; Yin, W.; Li, Q.; Wang, P.; Lu, Z.; Ma, J.; Han, H. *Biosens. Bioelectron.* **2017**, *92*, 321−327.
(42) Wen, W.; Huang, J. Y.; Bao, T.; Zhou, J.; Xia, H. X.; Zhang, X. H.; Wang, S. H.; Zhao, Y. D. *Biosens. Bioelectron.* **2016**, *83*, 142−148.
(43) Jiang, X.; Chen, K.; Wang, J.; Shao, K.; Fu, T.; Shao, F.; Lu, D.; Liang, J.; Foda, M. F.; Han, H. *Analyst* **2013**, *138*, 3388−3393.
(44) Wu, L.; Li, X.; Shao, K.; Ye, S.; Liu, C.; Zhang, C.; Han, H. *Anal. Chim. Acta* **2015**, *887*, 192−200.
(45) Pandit, K. R.; Nanayakkara, I. A.; Cao, W.; Raghavan, S. R.; White, I. M. *Anal. Chem.* **2015**, *87*, 11022−11029.
(46) Shao, K.; Wang, B.; Ye, S.; Zuo, Y.; Wu, L.; Li, Q.; Lu, Z.; Tan, X. C.; Han, H. *Anal. Chem.* **2016**, *88*, 8179−8187.
(47) Kang, X.; Wang, J.; Wu, H.; Aksay, I. A.; Liu, J.; Lin, Y. *Biosens. Bioelectron.* **2009**, *25*, 901−905.
(48) Cao, Y.; Zhu, S.; Yu, J.; Zhu, X.; Yin, Y.; Li, G. *Anal. Chem.* **2012**, *84*, 4314−4320.
(49) Jain, R.; Gupta, V. K.; Jadon, N.; Radhapyari, K. *Anal. Biochem.* **2010**, *407*, 79−88.

DOI: 10.1021/acs.analchem.7b01399
Anal. Chem. 2017, 89, 7578−7585